scientific reports

Check for updates

OPEN

Dysfunctional connectivity within hippocampal and entorhinal networks underlies early-life iron deficiency induced social recognition deficits, a preliminary study

Ao Ding[1,2,8], Ting Tan[2,6,8], Peng Liu[2,8], Xin Li[2,7], Mingwei Zhu[2], Hongsheng Liu[3], Ying Wang[4], Yuan Chen[1]✉ & Ya-Ping Tang[2,5]✉

Early-life iron deficiency (EID) has an adverse effect on cognition. Previous MRI studies revealed that EID could produce brain structural changes, while the significance remains elusive. To elucidate correlative functional changes is thus important. A low-iron diet feeding protocol was used to produce EID in rats, and a three-chamber test was used to evaluate social recognitions. T2-weighted and functional MRI (fMRI) were employed to conduct voxel-based morphometry (VBM) and voxel-wise functional connectivity (FC) analyses. Seed-based FC analyses were conducted, and based on the results, the hippocampus and entorhinal cortex (EC) were further respectively subdivided into 8 and 5 subregions, in order to perform deep seed-based FC analyses. EID rats were significantly impaired in social recognition. VBM analyses showed enlarged hippocampus and EC, and the FC between them was significantly decreased. Our deep seed-based analyses of FC further identified the impaired networks ($p < 0.001$, $q < 0.05$) between these two brain regions and between each of them and a number of other brain networks individually. All these results, although preliminarily, for the first time revealed the dysfunctional connectivity in three networks within the hippocampus and EC of the brain of EID rats, and may have a translational significance in early-diagnosis of EID.

Keywords Iron deficiency, Structural changes, Functional connectivity, MRI and fMRI, Hippocampus, Entorhinal cortex

Abbreviations

EID	Early life iron deficiency (EID)
FC	Functional connectivity
VBM	Voxel-based morphometry
rs-fMRI	Resting state of function MRI
ROIs	Regions of interest
CA1	Cornu ammonis 1

[1]Neurobiology Research Center, School of Medicine, Shenzhen Campus of Sun Yat-Sen University, Shenzhen 518107, China. [2]Guangzhou Women and Children's Medical Center, Guangzhou Institute of Pediatrics, Guangzhou Medical University, Guangzhou 510623, China. [3]Department of Radiology, Guangzhou Woman and Children's Medical Center, Guangzhou Medical University, Guangzhou 510623, China. [4]Department of Nuclear Medicine, The Fifth Affiliated Hospital, Sun Yat-sen University, Zhuhai 519000, China. [5]Institute of Neurological Disease, West China School of Medicine, Sichuan University, Sichuan University affiliated Chengdu Second People's Hospital, Chengdu 610041, China. [6] Institute of Neurological Disease, West China School of Medicine, Sichuan University, Sichuan University affiliated Chengdu Second People's Hospital, Chengdu 610041, China. [7] Institute of Neurological Disease, West China School of Medicine, Sichuan University, Sichuan University affiliated Chengdu Second People's Hospital, Chengdu 610041, China. [8]Ao Ding, Ting Tan and Peng Liu contributed equally to this work. ✉email: cheny33@mail.sysu.edu.cn; yptang12@126.com; yptang12@gzhmu.edu.cn

CA2	Cornu ammonis 2
CA3	Cornu ammonis 3
DG	Dentate gyrus
Fas-C	Fasciola cinereum
Para-SC	Parasubiculum
Pre-SC	Preasubiculum
SC	Subiculum
EC	Entorhinal cortex
LEC	Lateral entorhinal cortex
ep-LEC	Lateral entorhinal cortex external part
ip-LEC	Lateral entorhinal cortex internal part
MEC	Medial entorhinal cortex
PrL	Prelimbic cortex

Iron deficiency is one of the most common types of nutrient deficiency worldwide, and one of its most common sequela is iron deficiency anemia (IDA)[1]. The global prevalence of IDA was reported to be 30.2% among reproductive-aged women. In children, about 46–66% of them, younger than 4 years old suffer from anemia, in which half of these cases may attribute to early-life iron deficiency (EID)[1]. Obviously, EID represents a major disease-causative factor in anemia. There is robust evidence indicating that EID may adversely affect neuronal development, and consequently, impaired cognitive function mayrepresent its long-term effect[2]. As an essential nutrient, iron is needed for the synthesis of hemoglobin and myoglobin, and serves as a vital component or cofactor for numerous key enzymes, including cytochrome C reductase, tyrosine hydroxylase, and ribonucleotide reductase. The lack of hemoglobin may severely disrupt the supply of oxygen to the tissues, which is extremely harmful for the neuronal development. Furthermore, impairments of these enzymatic functions may disturb energy metabolisms, DNA synthesis, and especially protein syntheses[3]. All these disturbances may in turn severely disrupt neuronal development[3]. Indeed, there is evidence showing that human infants with EID suffer from compromised cognitive, motorial, and motional defects[4–8]. From the social-emotional domain viewpoint, EID infants may show more vigilance and hesitancy, reduced positive affectivity, diminished emotional responsiveness, excessive maternal proximity-seeking, and impaired social engagement[9–12]. Collectively, strong evidence from either basic research or clinical observations highlights the effects of EID on the development of disabilities in both emotion and social behaviors via disrupting the neuronal development[7].

It needs to be emphasized that the uses of MRI in human studies have led to many novel discoveries. For example, resting-state fMRI linked infantile iron deficiency to lifelong alterations in brain region network connectivity[13], T1-weighted volumetry uncovered paradoxical basal ganglia enlargement (left caudate/putamen, right putamen) inversely correlated with serum ferritin and psychiatric symptom severity[14], and quantitative susceptibility mapping (QSM)/relaxometry revealed significantly reduced brain iron content in ADHD children[15]. However, there are three issues that could interfere the interpretation. First, in those studies, a retrospective design was commonly adopted, which might produce many concerns in information collection, diagnostic criteria, the method used to monitor serum level of iron, etc. All these issues may constitute to a barrier for a precise analysis of the results. Second, it is almost impossible, either economically or ethically, to subject a patient for repeated MRI tests. Thus, the comparability, even within individual patients, is much lower. Lastly, in some longitudinal studies in humans, there might be a number of uncertain factors that may directly complicate the interpretations of the results, such as socioeconomic status, co-morbidities, and genetic background, etc[16]. These limitations may significantly devaluate the impact of those results in our efforts on establishing the neurobiological bases for the impaired cognitive function in EID.

Therefore, the uses of animal models is particularly important[2,17–19]. This is particularly true in our case, since our goal was to further explore the possible underlying molecular and histological mechanisms, which are ethically and practically impossible in the studies with human subjects. Actually, many previous studies did provide evidence showing how EID leads to changes, from neuronal development to behavioral abnormalities, including aberrant social behaviors[20–23].

One of the most important advantages in the uses of animal models is to be able to more precisely map brain regions that are affected by EID. At this stage, at least the prefrontal cortex, striatum, and hippocampus are currently considered as the key areas for EID-induced neural damages[24–27]. The neuronal activity within the hippocampal circuit is thought to be responsible for encoding social memories[22,23,28], pathological changes in this subcortical region might be underlie the social behavioral deficits observed in EID models. Within the hippocampal formation, the neuronal information is transduced by a sequential and unidirectional processing pattern, i.e. the information is first from the EC to the DG, then to the CA3 via mossy fibers, to the CA1via Schaffer collaterals, forming the classic tri-synaptic circuit (DG-CA3-CA1), and then the subiculum (SC), and ultimately returning to the EC through pre/para-subiculum (Pre/Para-SC)[29,30]. The EC, through its recurrent architectural organization, serves as a critical functional interface that integrates cortical inputs into the hippocampus via the DG-CA3-CA1-subicular pathway and relays processed hippocampal outputs to downstream cortical regions for behavioral modulation[29]. Collectively, this integrated circuitry enables the hippocampus to orchestrate multiple cognitive information, including acquisition and consolidation, recognition and spatial navigation, emotional regulation and memory association, and cognitive flexibility[28]. Notably, robust evidence identified hippocampal dysfunction as a key ingredient of EID-related brain impairments. Neonates with EID exhibit impaired hippocampus-mediated recognition memory[24,27]. Consistently with this, iron-deficient rats exhibited altered hippocampal energy metabolism, neurotransmission, myelination, dendritic architecture, and electrophysiological characteristics[24,27]. Furthermore, recent studies have also revealed that the hippocampus plays a pivotal role in social behaviors[22], particularly through the CA2-dependent social memory circuit and

DG-mediated context-dependent processing of social information[23]. Although many studies have focused on EID-induced structural changes in the brain, particularly in the hippocampus, few of them have evaluated functional relevance, such as FC etc[31–33]. For example, although the hippocampus was generally considered as a key brain region for social behaviors, most MRI studies on EID just focused on structural change, or changes at the biochemical composition level[31], few studies explored any possible functional alterations.

In this study, we established a rat model of EID to investigate the potential changes at both the structural and functional levels in the brain. We first employed whole-brain VBM and FC analyses to identify regions susceptible to EID, and based on the initial findings, we extended our studies into the FC in these brain areas. Specially, using deep seed-based analysis of the FC, we identified three networks within the hippocampus and EC. Our results have provided insightful information regarding how the EID affects functional networks in the brain.

Methods

Animals

Both male and female adult rats (Sprague-Dawley rats) were used throughout the experiments. Rats were purchased from the Charles River Laboratories (Beijing, China), and housed in an SPF animal facility in Guangzhou Women and Children's Medical Center (GWCMC)) under standard conditions (12 hr of light/dark cycle, temperature of 20–22 °C, humidity of 60%, and with food and water ad libitum). This study was reported in accordance with the ARRIVE guidelines. All the experiments were conducted in accordance with the animal care and use described in "Guidance for the Care and Use of Laboratory Animals" issued by National Science Foundation of China (NSFC), and were also pre-approved by the IACUC in GWCMC (Ethics No.2019–23001).

A paradigm of low-iron diet delivery was used to produce EID, and the details were described in elsewhere[17]. In brief, EID models were obtained from the pups whose dams were fed with iron deficiency (ID) diet (5 mg Fe/kg, RD18041204; ReadyDietech, Shenzhen, China) from the formation of plug up to weaning. Then, these pups were fed with the same ID diet up to the start of the experiments (5 week in age). Control animals were subjected to the same experimental procedures above, but the diet was replaced by a regular diet (RD) (200 mg Fe/kg, D10012G; ReadyDietech, Shenzhen, China). A total of 12 litters, respectively from 12 dams, and a total of 92 pups, were used. Within these 92 pups, 45 pups were EID models, and 47 ones were controls. The male/female ratio was 24/21 (1.14) in EID rats, and 23/24 (0.96) in controls. Pups from each dietary group were randomly allocated to different experiments: 20 pups for body weight monitoring, 11 pups for social/motor behavioral tests, 6 pups for immunofluorescent studies, and 6 pups for MRI studies in either EID or control group, respectively. No animals were reused across experiments to avoid carryover effects that could confound experimental results. The decision to use the animals at 5 weeks old is because of that at this stage, neuronal developments including myelination, refinement of neural circuitry, and fractionation/specialization of prefrontal cortex neural networks etc. are still undergoing[34]. Our experience and established literature indicating that: (1) behavioral testing can induce activity-dependent neural plasticity, which may alter brain states and confound subsequent imaging measurements[35]; and (2) anesthesia (e.g., isoflurane) required for MRI is itself a documented intervention that can impair social behavior and neural function, thereby affecting the validity of subsequent behavioral tests[36]. In addition, due to the nature of the social behavioral test used here, it is impossible to reuse animals in this kind of behavioral test. Based on all these rationals, we preferred to decrease the number of animals in each group, rather than to have a bigger sample size with some reused animals mixed, in order to have a more reliable conclusion. For tissue collection, animals were anesthetized with sodium pentobarbital (40 mg/kg, intraperitoneally), and transcardial perfusion was performed by using 0.9% saline, followed by 4% paraformaldehyde (PFA). For animals who needed to go over euthanasia, except for the same anesthetic procedures, but the dosage of sodium pentobarbital was 200 mg/kg, as described above, the death was confirmed by cervical dislocation.

As regarding to the guidance of NIH-announced Sex as a Biological Variable (SABV), the sample size, with mixed both sexes, in most conditions in our experiments met the requirement. In addition, in order to exclude any potential biased effect from animals with different sexes, we conducted multiple-way ANOVA analyses, in which the sex was treated as one independent factor. In a very few cases that the sample size was small ($n < 6$), a combined sex effect was determined. In the latter case, the potential limitations were discussed.

Behavioral assessments

To characterize behavioral alterations in the EID rats comprehensively, we conducted a series of behavioral assessments encompassing social interaction and motor function. . Experimenters who conducted the behavioral tests were blind to treatment of each animal until data analysis. Tests were conducted between 9:00–18:00 in a sound- and light-proof behavioral room. Four behavioral tests including the three-chamber test, rotarod, wire hanging, and grid walking were employed. In all these experiments, there were 11 animals in each group.

Three-chamber test

The method for the three-chamber test is outlined in our previous publication[37]. Throughout the experiment, rats were allowed unrestricted movement among the three designated areas. Initially, rats were allowed to freely explore all three zones for 10 min. For the next 10 min, a paper ball (non-social condition, NS) was positioned on one side of the area, while a target rat (social condition 1, S1) was placed on the opposite side of the enclosure. Thereafter, for an additional 10 min, the paper ball was substituted with another unfamiliar rat (social condition 2, S2). Video recordings were conducted using a digital camera and then analyzed using the SMART Video Tracking System (v3.0, Panlab Harvard Apparatus, Spain)[38] to determine the time in seconds (s) spent in each chamber across the three trials.

Rotarod

The rotarod experimental procedures are described elsewhere[39]. Briefly, rats were placed on a motorized cylinder, and the time the animals remained on the rungs was measured. The rotation speed was gradually accelerated from 4 to 40 rpm over 5 min (after an initial 1 min at 4 rpm). The experiment ended if the animal fell off the rungs or gripped the device and spun around for 2 consecutive revolutions without attempting to walk on the rungs.

Wire hanging

The wire hanging protocol is described elsewhere[40]. Briefly, the wire hanging test was conducted using a horizontally suspended metal bar (50 cm in length, 2 mm in diameter) affixed between two vertical poles. Animals were positioned with their forelimbs grasping the bar positioned 50 cm above a padded surface to ensure safety upon falling. Latency to fall (in seconds) was recorded from the moment of release until the animal lost its grip, with three consecutive trials performed per subject at ≥ 30-minute intervals to minimize fatigue interference. A predefined cutoff duration of 60 s was implemented to prevent physical exhaustion, and the mean latency across trials was calculated for statistical analysis.

Grid walking

The grid walking protocol was described elsewhere[41]. Briefly, rats were placed on an elevated metallic grid apparatus under standardized lighting for 2 min. While moving around on the grid, animals typically placed their paws on the wireframe for foot holds. Missteps were defined as limbs (forelimb or hindlimb) fully passing through grid openings during placement. Total steps (limb lifts typically placed on the wireframe) and missteps were quantified. The misstep ratio was calculated separately for forelimbs and hindlimbs.

Immunofluorescence staining

Immunofluorescence staining was conducted as previously described[42]. Briefly, rats were anesthetized and transcranial perfused with 0.9% saline, followed by 4% PFA. Dissected brain were fixed and equilibrated in 4% PFA in 30% sucrose phosphate buffer overnight. Coronal brain section (50 μm) were prepared using a cryostat (Leica 3050 S). Tissue sections were permeabilized with 0.3% Triton X-100 in phosphate buffered saline (PBS) and blocked with 5% goat serum in PBS containing 0.1% Triton X-100 for 1 h. Subsequently, brain sections were incubated with primary antibodies (IBA-1 antibody (1:1000; Abcam, ab178846), NeuN antibody (1:1000; Abcam, ab104224)) at 4 °C overnight, followed by incubation with fluorescent secondary antibodies (goat anti-rabbit IgG (Alexa Fluor 488; Abcam 150081) at 1:1000, goat anti-mouse IgG (Alexa Fluor 555; Abcam 150114) at 1:1000 fold-dilution) at room temperature for 1 hr. After washing, the slides were mounted with an anti-fade mounting medium (Electron Microscopy Sciences), and fluorescent images were captured using a microscopy system (Leica SP8). In all these experiments, there were 6 animals in each group.

MRI data acquisition

MRI imaging data were collected by using a 9.4 T MRI scanner (Biospec 94/30 USR, Bruker Biospin, Billerica, MA, USA). In each group, there were 6 animals. A volume transmits coil (86 mm inner diameter)[43] was used for radiofrequency excitation, and a rat head quadrature four-channel phased-array surface coil was used for signal reception[44].

The brain was carefully positioned at the isocenter a rigorous shimming procedure, global shimming followed by local shimming over an ellipsoidal volume covering the cerebrum using the MAPSHIM protocol (ParaVision, Bruker BioSpin)[45], which was implemented to ensure magnetic field homogeneity and mitigate potential signal loss in deeper structures (e.g., EC).

Rats were anesthetized with 3.5-4% isoflurane (ISO) in a mixture of medical-grade oxygen and medical air (3:7) delivered through a nose cone. After the loss of righting reflex responses, the ISO concentration was reduced to 2%, and a minimum stabilization period of 15–20 min was observed after reaching the desired anesthesia level before data acquisition[45]. During the acquisition, rats were placed in the scanning cradle with heads secured by ear plugs and a bite bar, and the body were fixed with the standard hospital tapes. The O_2/air/ISO (2%) mixture was continuously delivered at 1 L/min throughout the experiment[43], and physiological parameters were continuously monitored: respiration rate (maintained at 40–70 breaths per min) via a respiration pad, and body temperature (maintained at 37.0 ± 0.5 °C) with a combination of a warm-air heating system and a circulating warm-water blanket.

Structural signals were captured using the T2_TurboRARE sequence with parameters: TR/TE = 2000.000 ms/10.332 ms, field of view (FOV) = 30 × 21 mm^2, image size = 100 × 70 mm^2, and 45 slices with a slice thickness of 0.6 mm. The voxel size was 200 × 200 × 400 μm^3. BOLD signals were captured using the T2star_FID_EPI sequence and the following parameters: TR/TE = 4930.084 ms/21.59 ms, RARE factor 8, FOV = 30 × 21 mm^2, image size = 150 × 105 mm^2. 70 slices with 0.4 mm thickness were captured with voxel size of 300 × 300 × 600 μm^3. The scan lasted nearly 13 min. At the end of the scanning, rats were removed from the coil and returned to their cage.

Rs-fMRI data preprocessing and analysis

The first five volumes were discarded from each rs-fMRI run to ensure the steady state of the signal. rs-fMRI image preprocessing was conducted in Matlab (Mathworks, Natick, MA, USA) using SPM12 (http://www.fil.ion.ucl.ac.uk/spm/). The main preprocessing steps included slice timing, realignment, normalization to the SIGMA rat brain templates and atlases[46], and smoothing (FWHM = 0.8 mm).

To explore potential whole-brain structural alterations, we first performed VBM analysis on the high-resolution T2-weighted images. This process spatially normalizes the high-resolution T2-weighted images to the

same stereotaxic space, segmenting gray/white matter, smoothing and providing a voxel-by-voxel comparison of the local concentrations of gray matter in two groups[47].

Initial VBM analysis was conducted, and based on the results of VBM, we selected the hippocampus and the EC as regions of interest (ROIs), based on the fact that these areas represent hub nodes that function relevant to the social recognition deficits under study. To investigate whether the structural alterations revealed by VBM were associated with functional changes, a comprehensive whole-brain FC analysis was first performed. The integrated findings from both VBM and this whole-brain analysis motivated a subsequent voxel-wise FC mapping specifically for the hippocampus and EC. For both the whole-brain and voxel-wise FC mapping procedures, a whole-brain mask and ROI masks for the hippocampus and EC were defined based on the same brain atlases above. These analyses were then implemented using the DPABI toolbox[48]. Pearson correlation coefficients were examined for the average time series of the ROIs and all brain voxels to establish a seed-based voxel-wise functional connectivity map for the whole brain.

Subsequently to further test the hypothesis of subcircuit disruption within the hippocampal-entorhinal network, we subdivided the hippocampus and EC into 8 and 5 ROIs, respectively, i.e., CA1, CA2, CA3, DG, fasciola cinereum (Fas-C), Para-SC, Pre-SC, and SC, which are subregions of the hippocampus, and EC, LEC, ep-LEC, internal part of LEC (ip-LEC), and medial entorhinal cortex (MEC), which are subregions of the EC. In addition, the prelimbic cortex (PrL) was also included as an independent ROI to further investigate its potential role within the network, though it was not subdivided further, due to its relatively small size. These ROI-wise FC analyses were performed by defining all subregions by using the same rat brain atlases. For this analysis, Pearson correlation coefficients were examined for each pair of these ROIs to establish an ROI functional connectivity map using DPABI[48].

Statistical analyses

All data were first examined for their distribution (Shapiro-Wilk test) and homogeneity of variance (HGV; Levene's test). After the confirmation of normal distribution and HGV, data were then analyzed by using ANOVA or unpaired Student's *t* test, whereas it is appropriate. Data were expressed as mean ± SD, as those were indicated in each data set. A p-value < 0.05 was considered as significant differences. All these statistical analyses were performed by using SPSS (version 22.0). The detailed analyses were described in our Supplementary Materials.

Results

EID models in rats

The age of all the animals used was 5 weeks old. The decision of this age was based on the presumption that the effects of the EID on neuronal development in humans may last for a period of time crossing over from the prenatal stage up to the childhood or early adolescence, during which many neurodevelopmental procedures, such as synaptogenesis and maturation of the synapses etc. are still undergoing[34]. The age of 5 weeks in rodents is very equally to the age of 11–12 years old in human[34].

The overall condition, including eating behavior, body weight, and home-cage behavior were examined. A significant difference was neither noted in eating behavior nor in the general home-cage behavior. For the body weight, however, a significant reduction was observed in EID rats [$F(1,238) = 69.205$, $p < 0.001$]. *Post hoc* analysis revealed significant differences at P0 ($p = 0.004$), P7 ($p = 0.009$), P14 ($p = 0.008$), P21 ($p = 0.001$), P28 ($p < 0.001$), and P35 ($p < 0.001$) (Supplemental Fig. 1A). All these results indicated that the EID had a significantly negative effect on body weight gaining. A two-way ANOVA (Sex × Treatment) was performed to assess the potential influence of sex as a biological variable, and the result revealed no significant effect of Sex or Sex × Treatment in any level (the detailed statistical analysis of SABV is provided in our Supplemental Results under the title, "EID-induced body weight and brain weight changes are independent of sex in rats" in the Supplementary Materials). This indicated that the effect of EID on body weight was consistent between male and female pups. Therefore, data from both sexes were pooled in our analysis.

Despite this persistent effect on the growth rate, histological examination at P35 did not reveal any observable abnormalities at the cytoarchitectural or area-organizational levels of the brain between EID and control rats, the brain weight in EID rats was slightly, but not significantly, lower than that in control rats (EID: 1.400 ± 0.060 g vs. Control: 1.423 ± 0.063 g; $p = 0.245$, Supplemental Fig. 1B). Similarly, statistical analysis confirmed that this difference in brain weight was not influenced by sex, as no significant effect of Sex or Sex × Treatment interaction was found (see Supplemental Materials for details). These results suggested that the overall conditions, except for the body weight, were very similar between these two groups of rats.

EID rats were impaired in social recognition behaviors

To assess the potential influence of sex as a biological variable (SABV), a two-way ANOVA (sex × treatment) was performed from all behavioral tests. This analysis revealed no significant effect of sex or sex × treatment in any test (the detailed statistical analysis of SABV is provided in our Supplemental Results under the title, "EID-induced behavioral impairment is independent of sex in rats" in the Supplementary Materials). This indicated that the effects of EID on behavioral performance were consistent between male and female pups. Therefore, data from both sexes were pooled for subsequent analysis.

The travel trajectory of both the control and EID rats in the sociability phase of the three-chamber test was shown in Fig. 1A. As shown in Fig. 1B, quantitative analyses indicated that either the control rats [$F(1, 20) = 27.550$, $p < 0.001$] or EID rats [$F(1, 20) = 12.141$, $p = 0.002$] spent much less time in the empty chamber, compared to that in the chamber with a novel animal. However, there was no significant different in any chamber between control and EID rats. In the social novelty phase of the three-chamber test, however, the travel trajectory in control rats was obviously different from that in EID rats (Fig. 1C). Quantitative analyses revealed two significant differences between these two groups. The first one was a within-group difference in control rats

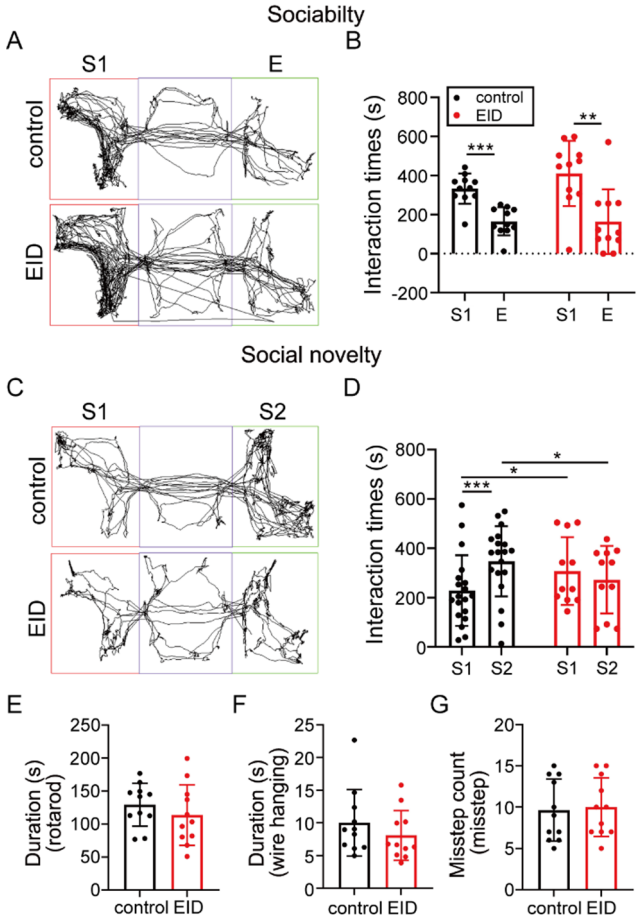

Fig. 1. EID rats exhibited impaired social recognition behaviors. (**A**) Trajectory maps from the sociability phase of the three-chamber test. (**B**) Quantification of the interaction time in the sociability phase (Stranger 1, S1 vs. Empty, E). (**C**) Trajectory maps from the social novelty phase. (**D**) Quantification of the interaction time in the social novelty phase (Stranger 2, S2 vs. Stranger 1, S1). (**E–G**). Motor function assessments by using the rotarod test revealed no significant differences between groups. In all these tests, $n = 11$. Data are presented as means ± SD, and *, $p < 0.05$; **, $p < 0.01$; ***, $p < 0.001$. One-way ANOVA was used to determine the effect on three-chamber test and motor function assessments.

[F(1, 20) = 23.879, $p < 0.001$], but not in EID rats, indicating that EID rats lost their social (face) recognition (Fig. 1D). The second one was a between-group difference in time-spent in S1 [F(1, 20) = 4.967, $p = 0.037$] or S2 chamber [F(1, 20) = 4.603, $p = 0.044$] between control and EID rats (Fig. 1D), further confirming the impaired socially recognitive function in EID rats.

In addition, motor function assessments in a rotarod test (balance/coordination), a wire hanging test (forelimb force), and a grid walking (gait stability) test were conducted to examine motor functions in EID rats. All the results from these tests revealed no deficits in motor function in EID rats, compared to that in control rats (Fig. 1E–G). Taken together, these results demonstrated that EID specifically disrupted the social recognition, and this deficit was not due to any motor dysfunction.

VBM revealed whole-brain structural changes in EID rats

VBM, a voxel-by-voxel comparison of gray matter concentration, was used to investigate structural changes at the whole-brain level (Fig. 2A). Following manual segmentation and strict quality control, one animal from the experimental group and three from the control group were excluded due to the poor image quality, resulting in a final size of 5 EID and 3 control animals for this analysis. Figure 2B shows a list of brain regions with the most significantly affected, according to VBM effect size in a formate of EID rats over control rats ($p < 0.001$; uncorrected). Figure 2C exhibits a fine display of both the hippocampus and EC, both of which were most significantly affected by EID: left hemisphere cluster size = 1877, peak MNI (− 64, − 61.1, 20.9), T(6) = 11.39, $p < 0.001$; right hemisphere cluster size = 1409, peak MNI (39, − 58.1, 46.4), T(6) = 10.37, $p < 0.001$.

Microglial activation, but not neuronal loss, underlies structural alterations

The results from MRI studies above manifested the brain structural changes in both the hippocampus and EC in EID rats at a gross level. We further employed immunofluorescence and histological staining to detect whethere there were any changes at the fine anatomical level.

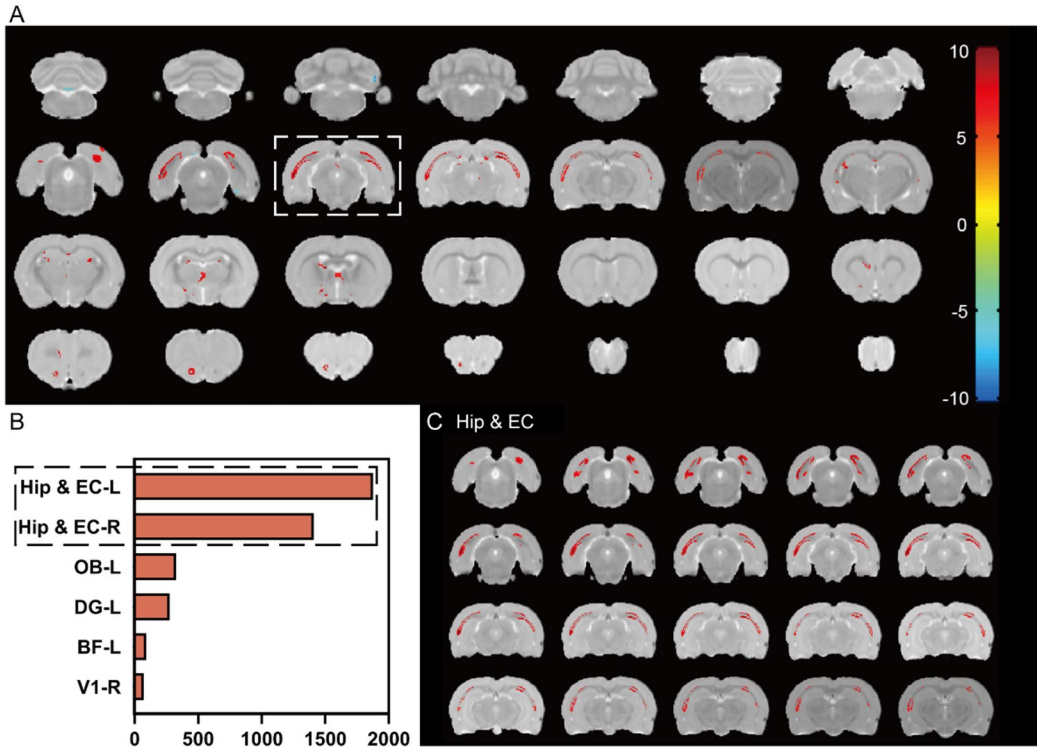

Fig. 2. VBM revealed whole-brain structural changes in EID rats. (**A**) an overview of structural changes in a formate of EID rats over control rats at the whole-brain level detected by VBM ($p = 0.001$, cluster level uncorrected; control group $n = 3$, EID group $n = 5$). (**B**) VBM identified regions with most significant differences, ranked based on VBM effect size from largest to smallest. (**C**) A fine display of the biggest regions of the VBM effect size report (left hemisphere cluster size = 1877; right hemisphere cluster size = 1409). The hippocampus and EC are shown together as they formed a continuous cluster of alteration. All Student's *t* tests.

The effects on neuronal and microglial markers in the hippocampus and EC were assessed by immunohistochemistry. Supplemental Fig. 2A and 3 A show a representative comparison between a VBM picture and an immunofluorescence-stained brain section at the same level. As illustrated in Supplemental Fig. 2B-E, representative photos of NeuN (Supplemental Fig. 2B) and their quantitative analyses (Supplemental Fig. 2C) were presented alongside those for IBA-1 (Supplemental Fig. 2D and E, respectively). An identical analysis for the EC region was detailed in Supplemental Fig. 3B–E, Supplemental Fig. 3B and C presented NeuN staining and analysis, while Supplemental Fig. 3D and E showed the corresponding IBA-1 data. Unexpectedly, NeuN staining did not reveal a significant difference in neuron number in the hippocampus or EC between the control and EID rats. However, staining with IBA-1, a marker for microglia cells, did demonstrate a significantly higher expression level in the hippocampus ($p = 0.006$) and EC ($p = 0.002$) in EID rats, respectively compared to that in control rats.

Taken together, these results suggest that the macro-scale structural alterations observed with VBM are unlikely to be driven by neuronal loss. Instead, they may be related to a pronounced neuroimmune response, as indicated by microglial activation. This provides a potential cellular mechanism underlying the MRI-observed changes and confirms an adverse effect of EID on neurodevelopment.

Rs-fMRI revealed impaired FC in hippocampus-EC network, and hippocampus/ EC-PrL networks in EID rats

Via evaluating the VBM, we found that the most significantly structural changes were located in the hippocampus and EC of EID rats. The T2 structural data were integrated with corresponding BOLD signals and rs-fMRI analysis was conducted to determine whether the structural modifications correlated with functional alterations. Following quality assessments, one animal from the control group was excluded from the subsequent functional analyses due to its poor BOLD signal quality, resulting in a final size of the animals was 6 in EID and 5 in control animals. A comprehensive whole-brain functional connectivity analysis was performed to systematically map neural network in the brain.

The overview of voxel-wise functional connectivity analysis conducted at the whole-brain level is shown in Fig. 3A. Figure 3B illustrates the detailed cluster location which were most significantly different, according to voxel-wise FC in a formate of EID rats over control rats ($p = 0.01$; uncorrected). Figure 3C provides a fine display of the most significant cluster affected by EID. rs-fMRI analysis showed the whole-brain level FC was decreased with greatest reduction noted in the hippocampus and EC: left hemisphere cluster size = 610, peak MNI (− 75, − 63, 6), T(9) = − 8.54, $p < 0.001$; right hemisphere cluster size = 412, peak MNI (72, − 66, 3), T(9) = − 6.01,

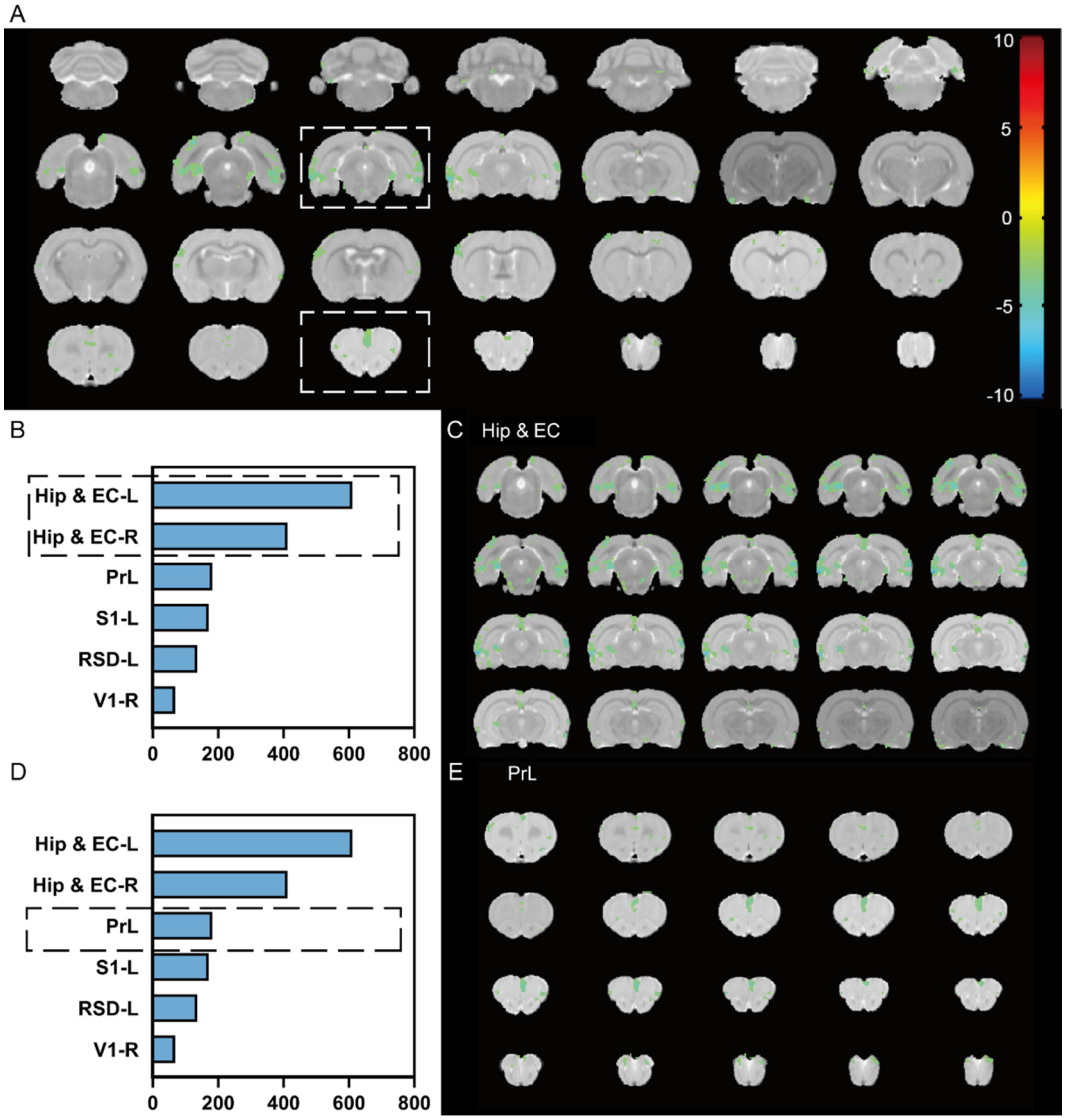

Fig. 3. Whole-brain level voxel-wise functional connectivity showed dysfunctional connectivity in EID rats. (**A**) An overview of the FC mapping conducted at the whole-brain level in a formate of EID rats over control rats ($p = 0.01$, cluster level uncorrected; control group $n = 5$, EID group $n = 6$). (**B**) Brain regions reported with most significant differences, ranked based on voxel size of the FC changes from largest to smallest. (**C**) A fine display of the biggest regions of the FC voxel size report in whole-brain level (left hemisphere cluster size = 610; right hemisphere cluster size = 412). (**D**) Brain regions reported with most significant differences, specifically pointed PrL, which ranked in the third. (**E**) A fine display of the PrL with a combined cluster size of 182 voxels in both hemispheres. The hippocampus and EC are shown together as they formed a continuous cluster of alteration. All Student's *t* test.

$p < 0.001$ in the EID over to control rats. Notably, the PrL, a key cortical region and a recipient of hippocampal projections regulating social behavior, exhibited significantly reduced FC: peak MNI (3, 54, 42), T(9) = − 5.44, $p < 0.001$, with the combined bilateral cluster size of 182 voxels.

An integrated analysis of the findings from VBM and whole-brain FC motivated us to select the hippocampus and EC as ROI for voxel-wise FC mapping. Figure 4A shows the seed-based analyses mapping of the hippocampus also in the formate of EID rats over control rats, which further documented that the decrease in FC was particularly noted in the hippocampus and EC: left hemisphere cluster size = 640 voxels, peak MNI (− 75, − 54, 6), T(9) = − 5.90, $p < 0.001$, right hemisphere cluster size = 501 voxels, peak MNI (63, − 72, 3), T(9) = − 6.26, $p < 0.001$; (Fig. 4B-C), and in other brain regions, such as PrL also: bilateral cluster size = 13 voxels; peak MNI (0, 45, 36), T(9) = − 3.37, $p = 0.008$ (Fig. 4D–E).

Our further FC examination that encompassed EC as ROI showed results consistent with those obtained from the hippocampus-based analysis, with the decreased and the greatest reduction in FC was found in the hippocampus and EC: left hemisphere cluster size = 476, peak MNI (− 75, −57, 3), T(9) = − 5.76, $p < 0.001$; right hemisphere cluster size = 371, peak MNI (72, − 66, 3),T(9) = − 5.12, $p < 0.001$ in the EID over control animals

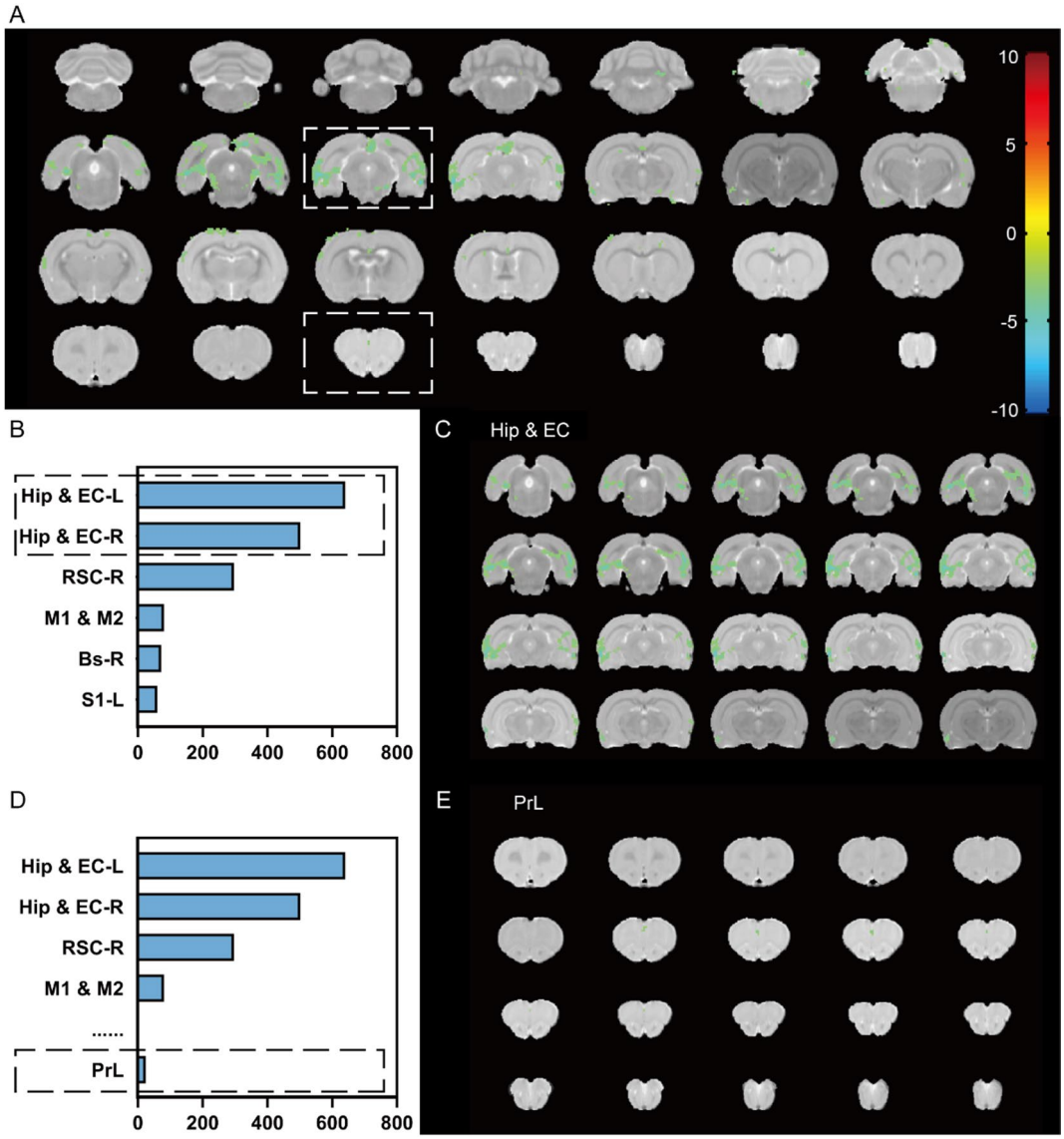

Fig. 4. Voxel-wise functional connectivity showed dysfunctional connectivity at hippocampus in EID rats. (**A**) An overview of the FC changes at hippocampus in a formate of EID rats over control rats. ($p = 0.01$, cluster level uncorrected; control group $n = 5$, EID group $n = 6$). (**B**) Brain regions reported with most significant differences, ranked based on voxel size of the FC changes from largest to smallest. (**C**) A fine display of the biggest regions of the FC voxel size report in hippocampus (left hemisphere cluster size = 640 voxels; right hemisphere cluster size = 501 voxels). (**D**) Brain regions reported with most significant differences, specifically pointed PrL. (**E**) A fine display of the PrL with a combined cluster size of 13 voxels in both hemispheres. The hippocampus and entorhinal cortex are shown together as they formed a continuous cluster of alteration. All Student's *t* test.

(Figs. 5A–C). Figure 5D–E presents detailed spatial localization and a high-resolution visualization of the PrL. The rs-fMRI analysis identified significantly reduced functional connectivity in this region: peak MNI (0, 45, 36), $T(9) = -4.43$, $p = 0.002$, in the EID over the control group with a combined cluster size of 135 voxels in both hemispheres.

Taken together, our results revealed a significant disruption of FC within the hippocampus or EC itself, and more importantly, between these two critical brain regions. Furthermore, a decreased connectivity between the hippocampus and PrL, and especially between the EC and PrL, were also exceptional. Clearly, these results have pointed to a potentially novel neural mechanism at the FC level for the EID-induced deficits in social behaviors.

Deep features in dysfunctional connections within neural circuitries identified above in EID rats

Although our results above did establish the dysfunctional connections among three key brain regions, it must be more interest to eventually figure out the dis-connective architecture within each individual brain region/

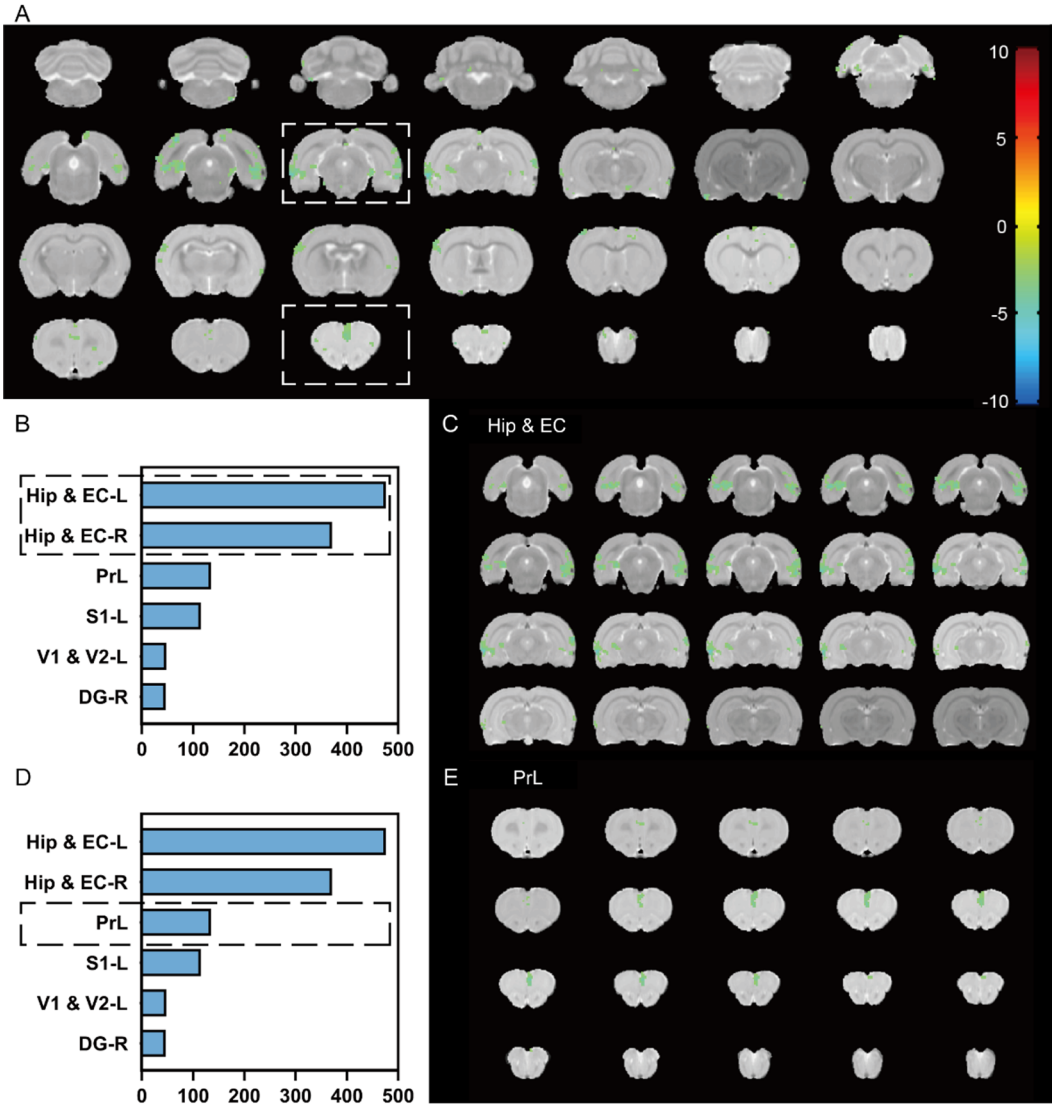

Fig. 5. Voxel FC showed dysfunctional connectivity at EC in EID rats. (**A**) An overview of the FC changes at EC in a formate of EID rats over control rats. ($p = 0.01$, cluster level uncorrected; control group $n = 5$, EID group $n = 6$). (**B**) Brain regions reported with most significant differences, ranked based on voxel size of the FC changes from largest to smallest. (**C**) A fine display of the biggest regions of the FC voxel size report in EC (left hemisphere cluster size = 476 voxels; right hemisphere cluster size = 371 voxels). (**D**) Brain regions reported with most significant differences, specifically pointed PrL, which ranked in the third. (**E**) A fine display of the PrL with a combined cluster size of 135 voxels in both hemispheres. The hippocampus and entorhinal cortex are shown together as they formed a continuous cluster of alteration. All by Student's *t*-tests.

neuronal circuity. To this end, we subjected the hippocampus, EC, and PrL as an independent ROIs, and further sub-divided the hippocampus into 8 and EC into 5 subregions. The PrL remained as a single region, due to its small size. Following rigorous denoising, one additional control animal was excluded, yielding a final sample size to be 6 in EID, and 4 in control rats.

Based on these 14 ROIs, we performed ROI-wise FC analysis. Figure 6A, shows a heatmap of significantly changed FC between two regions across these 14 ROIs, threshold at three significance levels (blue: $p < 0.05$; gray: $p < 0.01$; red: $p < 0.001$, uncorrected). However, for subsequent analyses, a more stringent threshold was applied; only connections surviving a significance level of $p < 0.001$ and FDR correction ($q < 0.05$) were considered statistically robust and were therefore selected for further investigation, but we still showed a result of $p < 0.01$. The most severe functional disruptions were notable between the hippocampus and EC [$T(8) = -8.56$, $p < 0.001$, FDR $q = 0.00243$ in DG-LEC; and $T(8) = -6.38$, $p < 0.001$, FDR $q = 0.00975$ in SC-LEC], with an additional disruption observed within the EC [$T(8) = -5.17$, $p < 0.001$, FDR $q = 0.026$, in ep-LEC-LEC]. Within the PrL, regional dysfunction did not reach the predefined significance threshold ($p < 0.001$, FDR < 0.05), whereas FC between the PrL and LEC did show a significant reduction ($p = 0.004$). Figure 6C illustrates the T-value circular graph across the whole brain regions and further confirming that the LEC exhibited the highest number of dysfunctional connectivity, and the areas or circuitries that were affected included the DG, CA1, Fas-C; SC and

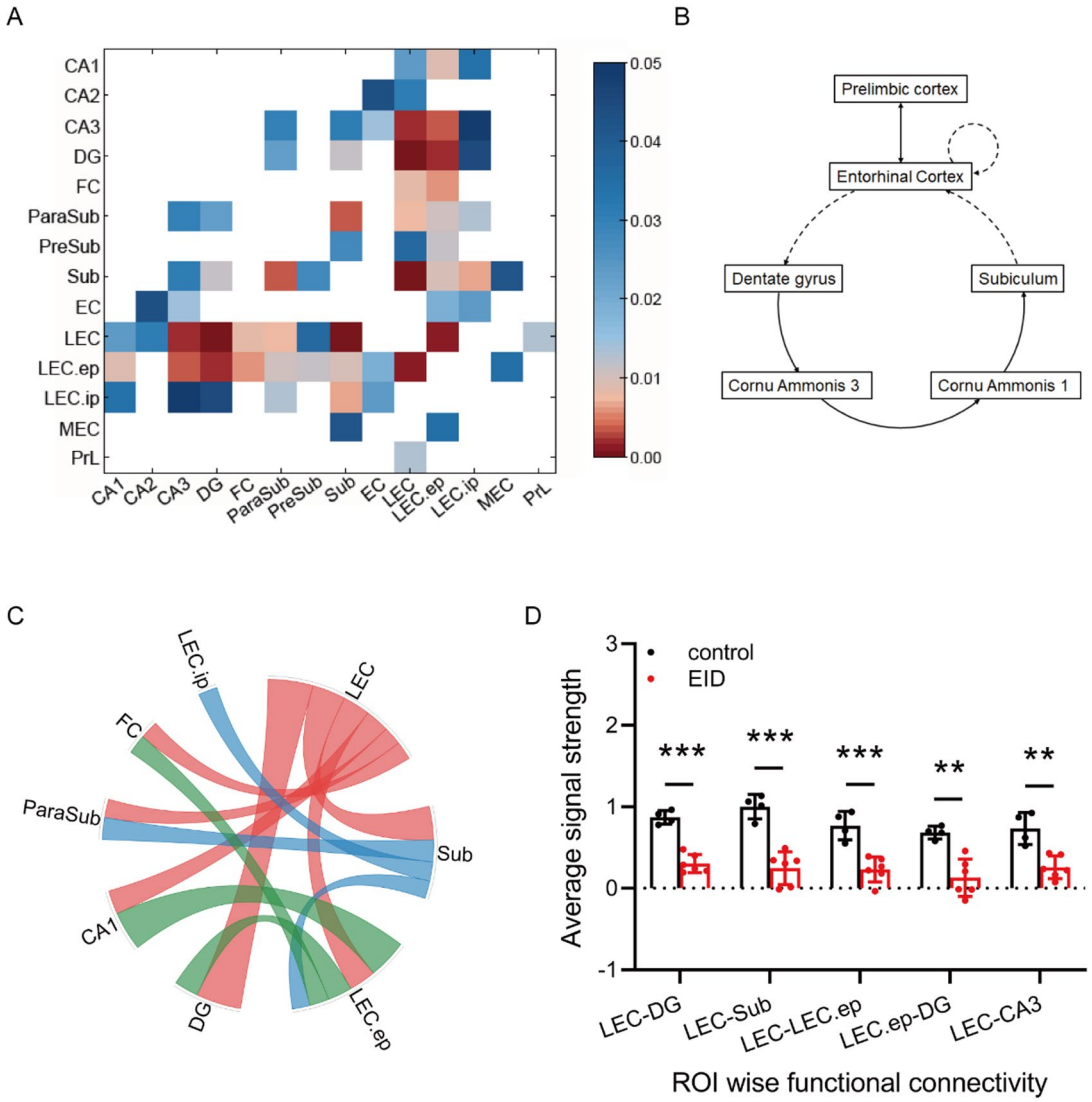

Fig. 6. Deep features in dysfunctional connections within neural circuitries identified above in EID rats. (**A**) The p-value heat map of the ROI functional connectivity result ($p < 0.05$- $p < 0.001$; control group $n = 4$, EID group $n = 6$); (**B**) The pattern of cortical and intrinsic connectivity of the hippocampal formation changes between control and EID groups. Solid lines represent neural pathways with intact functional connectivity in EID, including the classic tri-synaptic circuit (DG-CA3-CA1). Dashed lines represent pathways that exhibited a significant reduction in functional connectivity in the EID group compared to controls ($p < 0.001$, FDR $q < 0.05$); (**C**) The circular graph of the ROI functional connectivity results ($p < 0.01$); (**D**) Functional connectivity changes reported according to the p-value on ordering from largest to smallest (for DG-LEC, control: $M = 0.87$, $SD = 0.08$; EID: $M = 0.30$, $SD = 0.11$, $t(8) = -8.56$, $p < 0.001$; for Sub-LEC control: $M = 1.00$, $SD = 0.15$; EID: $M = 0.25$, $SD = 0.20$, $t(8) = -6.38$, $p < 0.001$; for LEC.ep-LEC, control: $M = 0.77$, $SD = 0.17$; EID: $M = 0.23$, $SD = 0.15$, $t(8) = -5.17$, $p < 0.001$). All data in bar figures are presented as mean ± SD, and *, $p < 0.05$; **, $p < 0.01$; ***, $p < 0.001$, all by unpaired two-tailed Student's t-tests.

Para-SC within the hippocampus, and ip-LEC and ep-LEC within the EC. Figure 6D shows 5 FCs that were most significantly disrupted, and these FCs were between LEC and DG, SC and LEC, ep-LEC and LEC, ep-LEC and DG, and LEC and CA3. All these results indicated that dysfunctional networks between the hippocampus and EC may underly EID-induced deficit in social recognition.

Discussion

In this study, we demonstrated, for the first time, that functional disruption in the EC and hippocampus may be fundamentally critical for the development of EID-induced deficits in social recognition. Specifically, the EC, as a critical region for bidirectional information processing between the hippocampus and PrL, exhibited both impaired information transferring capacity and intrinsically functional abnormalities. In addition, we manifested a potential association between structural changes in the hippocampus and the increased numbers

of microglia. All these results provide an insight into the neuronal mechanism underlying the deficits in social recognition that was associated with EID.

There are several strengths to our study. First, multiple behavioral tests were conducted to demonstrate that EID selectively impaired social recognition behaviors, and this phenotype was independent of motor dysfunction. Second, multimodal neuroimaging approaches systematically identified the critical involvement among the hippocampus, EC and PrL as potential brain regions associated with the observed phenotypes. Finally, deep features in dysfunctional connections, were analyzed by subdividing these regions into 14 subdomains revealed that dysconnectivity between hippocampus and EC and within the EC might underlie EID-induced deficits in social recognition.

The most striking finding in this study was the finding that the disrupted FC between the hippocampus and EC and within the EC, as revealed by ROI-wise FC analysis, was demonstrated. As shown in the schematic (Fig. 6B), our ROI-wise FC analysis visually summarized that solid lines represent pathways with preserved connectivity in EID, including the classic tri-synaptic circuit (DG→CA3→CA1) within the hippocampus. In contrast, dashed lines represent pathways exhibiting a severe and significant impairment in functional connectivity. Specifically, severe deficits not only between the hippocampus and EC ($p < 0.001$, FDR $q < 0.05$ in DG - LEC, and SC-LEC), but also within the EC itself ($p < 0.001$; FDR $q < 0.05$ for ep-LEC-LEC; Fig. 6A-D). In prior studies, the EC was recognized as a critical functional interface due to its recurrent architecture, which integrates cortical inputs into the hippocampus via the DG and relays processed hippocampal outputs from the SC to downstream cortical regions[29]. Taken together, our multimodal connectivity analyses demonstrated that EID-induced social recognition deficits arise from dysfunctional hippocampal-EC networks, providing a new mechanistic in FC level explanation for the neurodevelopmental consequences of EID.

Another important finding in this study was that our whole-brain voxel-wise FC analysis revealed decreased FC in EID animals, with the most significantly reductions localized to the hippocampus and EC. Notably, the PrL also exhibited significant FC decreases (bilateral cluster size = 182 voxels; Fig. 3D–E). Consistent with these findings, seed-based analyses using hippocampal and EC as ROIs demonstrated similar results, a decreased connectivity between the hippocampus and PrL (bilateral cluster size = 24 voxels; Fig. 4D–E), and especially between the EC and PrL(bilateral cluster size = 135 voxels; Fig. 5D–E), were also exceptional. According to the literature, hippocampal-prefrontal connectivity was mediated by EC in humans[29], whereas animal studies had identified direct hippocampal-PrL projections[49]. Additionally, studies had shown that the hippocampus and PrL were both involved in changes in social behavior[50,51]. These findings emphasized the need to elucidate the disconnection architecture within specific brain regions and their associated neuronal circuits. Subsequent subregions ROI-wise FC did identify the regional dysfunction appeared between PrL and the EC subregion LEC ($p = 0.004$). However, this finding fell below the predefined significance threshold ($p < 0.001$; FDR $q < 0.05$). These results suggest that although functional disconnections between the EC and PrL might contribute to behavioral deficits, the primary mechanistic driver of EID-induced social recognition impairments might underlie disrupted hippocampal-EC network dysfunction.

It should be mentioned that in our studies, VBM density in the brain, especially in the hippocampus, of EID rats was significantly increased, while in previous study, it was reported that the hippocampal volume was decreased following EID[31]. This discrepancy may be due a couple of reasons. Firstly, the age of animals examined was different. In our case, the age was much younger than the others, which may raise an issue regarding if the results obtained were reflecting for a relatively short-term vs. relatively long-term effect of EID. Secondly, evaluating methods used were different. In their case, hippocampal volume was measured using a RARE sequence-based MRI with presumed T2-weighted contrast, with a focus on volume changes only. In our cases, however, the VBM, an evaluating method focused on the local concentrations of gray matter was used, which might detect the potential changes from a different angle. Lastly, concentration and volume are not simply comparable, and thus, these two indices might tell different aspects of pathology that is associated with EID.

There was another issue that we need to discuss. Despite that we found the structural changes in the brain of EID rats, we could not demonstrate these changes at the gross histological level. As shown in Supplemental Fig. 2B-C and Supplemental Fig. 3B-C, our NeuN-staining showed that there was no significant difference in neuron numbers in the hippocampus or EC between control and EID rats. Actually, in other studies, the histological changes were also only found at the dendritic or synaptic levels[52,53]. In our studies, however, an interesting, and potentially very important finding was demonstrated. As shown in Supplemental Fig. 2D-E and Supplemental Fig. 3D-E, the expression of IBA-1, a marker for microglia cells, was significantly increased in the hippocampus and EC of EID rats. This microglial activation aligns with other study demonstrating that developmental IDA induces persistent dysregulation of neuroinflammation-related genes in the hippocampus of rats, suggesting activation of microglia[54]. Microglia cells are broadly involved in inflammatory responses in the brain[32,33]. Overactivation of this type of cells definitely means that there much be somewhat damages happen onsite. Therefore, our results from a more explainable way demonstrated harmful effect of EID on the neuronal system.

It should be mentioned that one limitation in this study was the sample size that used for MRI experiments was relatively small. This limitation may have two negative impacts for our study. First, the small sample size significantly hampered our statistical analyses in VBM and voxel-wise FC. Although our results reached the significant level at the voxel-level, but could not pass the cluster-level. Very fortunately, however, our results in deep seed-based analyses of FC exhibited a significant FDR level. We need to point out, under such a condition of small sample size, the positive results in our deep seed-based analyses of FC suggested two significances. The first one was that the difference was indeed obviously, and second, the identified intraregional networks might be of really high impact for our further understanding of how the EID causes behavioral deficit in social engagement. Second, the small sample size made us difficult to elucidate the potential sex effect, based on the regulations from SABV. Although we did not find any significant sex effect on our behavioral analyses, we could proof this is true in our MRI experiments such as VBM and voxel-wise FC. Again, our results in deep seed-based

analyses of FC seemed to be able to at least partially defense this potential defect. In addition, the mechanism underlying the neuroinflammation remains to be further explored, as this we did not address in the current study. We do plan to continue this investigation in our future work.

In summary, our findings highlighted the potentially more prominent role of the EC in EID-associated changes in behavior, which may provide novel insights into the mechanisms underlying EID-induced hippocampal structural and functional alterations. MRI techniques were employed to obtain novel insights into EID-related hippocampal dysfunction in rats, establishing this potential clinical application of MRI in children with EID. The demonstration of detrimental effects and hippocampal impairments highlight the importance of preventing perinatal EID in high-risk populations.

Data availability

All data generated or analyzed for this study are included in this published article and its supplementary information files.

Received: 6 June 2025; Accepted: 14 January 2026
Published online: 28 January 2026

References

1. Cappellini, M. D., Santini, V., Braxs, C. & Shander, A. Iron metabolism and iron deficiency anemia in women. *Fertil. Steril.* **118**(4), 607–614 (2022).
2. Lozoff, B. & Georgieff, M. K. Iron deficiency and brain development. *Semin Pediatr. Neurol.* **13**(3), 158–165 (2006).
3. Beard, J. L. Iron biology in immune Function, muscle metabolism and neuronal functioning. *J. Nutr.* **131**(2), 568S–580S (2001).
4. Lozoff, B. Early iron deficiency has brain and behavior effects consistent with dopaminergic Dysfunction1–3. *J. Nutr.* **141**(4), 740S–746S (2011).
5. Grantham-McGregor, S. & Ani, C. A review of studies on the effect of iron deficiency on cognitive development in children. *J. Nutr.* **131**(2), 649S–668S (2001).
6. McCann, J. C. & Ames, B. N. An overview of evidence for a causal relation between iron deficiency during development and deficits in cognitive or behavioral function. *Am. J. Clin. Nutr.* **85**(4), 931–945 (2007).
7. Lozoff, B. Iron deficiency and child development. *Food Nutr. Bull.* **28**(4_suppl4), S560–S571 (2007).
8. Sachdev, H., Gera, T. & Nestel, P. Effect of iron supplementation on mental and motor development in children: systematic review of randomised controlled trials. *Public. Health Nutr.* **8**(2), 117–132 (2005).
9. Lozoff, B. et al. Behavior of infants with iron-deficiency anemia. *Child. Dev.* **69**(1), 24–36 (1998).
10. Lozoff, B. et al. Dose-response relationships between iron deficiency with or without anemia and infant social-emotional behavior. *J. Pediatr.* **152**(5), 696–702 (2008). 702.31-33.
11. Oski, F. A., Honig, A. S., Helu, B. & Howanitz, P. Effect of iron therapy on behavior performance in nonanemic, iron-deficient infants. *Pediatrics* **71**(6), 877–880 (1983).
12. Honig, A. S., Oski, F. A., Solemnity & A clinical risk index for iron deficient infants. *Early Child. Dev. Care.* **16**(1–2), 69–83 (1984).
13. Algarin,C. et al. Differences on brain connectivity in adulthood are present in subjects with iron deficiency anemia in infancy. *Front. Aging Neurosci.* **9**, 54. https://doi.org/10.3389/fnagi.2017.00054 (2017).
14. Abbas, M., Gandy, K., Salas, R., Devaraj, S. & Calarge, C. A. Iron deficiency and internalizing symptom severity in unmedicated adolescents: a pilot study. *Psychol. Med.* **53**(6), 2274–2284 (2023).
15. Morandini, H. A. E., Watson, P. A., Barbaro, P. & Rao, P. Brain iron concentration in childhood ADHD: A systematic review of neuroimaging studies. *J. Psychiatr. Res.* **173**, 200–209 (2024).
16. Schmidt, R. J., Tancredi, D. J., Krakowiak, P., Hansen, R. L. & Ozonoff, S. Maternal intake of supplemental iron and risk of autism spectrum disorder. *Am. J. Epidemiol.* **180**(9), 890–900 (2014).
17. Liu, S. X. et al. Prenatal iron deficiency and choline supplementation interact to epigenetically regulate Jarid1b and Bdnf in the rat hippocampus into adulthood. *Nutrients* **13**(12), 4527 (2021).
18. Kennedy, B. C. et al. Beneficial effects of postnatal choline supplementation on long-Term neurocognitive deficit resulting from fetal-Neonatal iron deficiency. *Behav. Brain. Res.* **336**, 40–43 (2018).
19. Tran, P. V., Fretham, S. J. B., Wobken, J., Miller, B. S. & Georgieff, M. K. Gestational-neonatal iron deficiency suppresses and iron treatment reactivates IGF signaling in developing rat hippocampus. *Am. J. Physiology-Endocrinology Metabolism.* **302**(3), E316–E324 (2012).
20. Youdim, M. B. H., Zamir, N. & Yehuda, S. The involvement of enkephalin system in analgesia induced by brain iron deficiency. *Nutr. Neurosci.* **3**(5), 357–365 (2000).
21. Yehuda, S. & Youdim, M. B. Brain iron: a lesson from animal models. *Am. J. Clin. Nutr.* **50**(3), 618–629 (1989).
22. Montagrin, A., Saiote, C. & Schiller, D. The social hippocampus. *Hippocampus* **28**(9), 672–679 (2018).
23. Chen, S. et al. A hypothalamic novelty signal modulates hippocampal memory. *Nature* **586**(7828), 270–274 (2020).
24. Ortiz, E. et al. Effect of manipulation of iron storage, transport, or availability on Myelin composition and brain iron content in three different animal models. *J. Neurosci. Res.* **77**(5), 681–689 (2004).
25. Ward, K. L. et al. Gestational and lactational iron deficiency alters the developing striatal metabolome and associated behaviors in young Rats1. *J. Nutr.* **137**(4), 1043–1049 (2007).
26. Carlson, E. S. et al. Iron is essential for neuron development and memory function in mouse hippocampus. *J. Nutr.* **139**(4), 672–679 (2009).
27. Li, Y. et al. Severe postnatal iron deficiency alters emotional behavior and dopamine levels in the prefrontal cortex of young male rats. *J. Nutr.* **141**(12), 2133–2138 (2011).
28. Douglas, R. J. The hippocampus and behavior. *Psychol. Bull.* **67**(6), 416–442 (1967).
29. Schultz,C. & Engelhardt, M. Anatomy of the hippocampal formation. *Front. Neurol. Neurosci.* **34**, 6–17. https://doi.org/10.1159/000360925 (2014).
30. Qiu, S. et al. Whole-brain Spatial organization of hippocampal single-neuron projectomes. *Science* **383**(6682), eadj9198 (2024).
31. Mudd, A. et al. Early-Life iron deficiency reduces brain iron content and alters brain tissue composition despite iron repletion: A neuroimaging assessment. *Nutrients* **10**(2), 135 (2018).
32. Fitch, M. T. & Silver, J. CNS injury, glial scars, and inflammation: inhibitory extracellular matrices and regeneration failure. *Exp. Neurol.* **209**(2), 294–301 (2008).
33. Mesquida-Veny, F., Del Río, J. A. & Hervera, A. Macrophagic and microglial complexity after neuronal injury. *Prog Neurobiol.* **200**, 101970 (2021).
34. Semple, B. D., Blomgren, K., Gimlin, K., Ferriero, D. M. & Noble-Haeusslein, L. J. Brain development in rodents and humans: identifying benchmarks of maturation and vulnerability to injury across species. *Prog. Neurobiol.* **106–107**, 1–16 (2013).

35. Aye, N. et al. Longitudinal changes of quantitative brain tissue properties induced by balance training. *Hum. Brain. Mapp.* **46**(4), e70128 (2025).
36. He, M. et al. Structural basis for the Inhibition of cystathionine-β-synthase by isoflurane and its role in anaesthesia-induced social dysfunction in mice. *Br. J. Anaesth.* **134**(3), 746–758 (2025).
37. Wang, X. et al. Maternal diabetes induces autism-like behavior by hyperglycemia-mediated persistent oxidative stress and suppression of superoxide dismutase 2. *Proc. Natl. Acad. Sci. U S A.* **116**(47), 23743–23752 (2019).
38. Li, W. et al. Behavioral abnormalities and phosphorylation deficits of extracellular signal-regulated kinases 1 and 2 in rat offspring of the maternal immune activation model. *Physiol. Behav.* **217**, 112805 (2020).
39. Shiotsuki, H. et al. A Rotarod test for evaluation of motor skill learning. *J. Neurosci. Methods*. **189**(2), 180–185 (2010).
40. Liu, H. et al. Scalp acupuncture attenuates neurological deficits in a rat model of hemorrhagic stroke. *Complement. Ther. Med.* **32**, 85–90 (2017).
41. Liu, Z. et al. Subacute intranasal administration of tissue plasminogen activator increases functional recovery and axonal remodeling after stroke in rats. *Neurobiol. Dis.* **45**(2), 804–809 (2012).
42. Chen, Q. et al. Adult neurogenesis is functionally associated with AD-like neurodegeneration. *Neurobiol. Dis.* **29**(2), 316–326 (2008).
43. Jung, W. B., Shim, H. J. & Kim, S. G. Mouse BOLD fMRI at ultrahigh field detects somatosensory networks including thalamic nuclei. *NeuroImage* **195**, 203–214 (2019).
44. Serres, S. et al. Structural and functional effects of metastases in rat brain determined by multimodal MRI. *Int. J. Cancer*. **134**(4), 885–896 (2014).
45. Le, T. T., Im, G. H., Lee, C. H., Choi, S. H. & Kim, S. G. Mapping cerebral perfusion in mice under various anesthesia levels using highly sensitive BOLD MRI with transient hypoxia. *Sci. Adv.* **10**(9), eadm7605 (2024).
46. Barrière, D. A. et al. The SIGMA rat brain templates and atlases for multimodal MRI data analysis and visualization. *Nat. Commun.* **10**(1), 5699 (2019).
47. Ashburner, J. & Friston, K. J. *Voxel-Based Morphometry—The Methods NeuroImage* ;**11**(6):805–821. (2000).
48. Yan, C. G., Wang, X. D., Zuo, X. N. & Zang, Y. F. DPABI: data processing & analysis for (Resting-State). *Brain Imaging Neuroinform.* **14**(3), 339–351 (2016).
49. Ye, X., Kapeller-Libermann, D., Travaglia, A., Inda, M. C. & Alberini, C. M. Direct dorsal hippocampal–prelimbic cortex connections strengthen fear memories. *Nat. Neurosci.* **20**(1), 52–61 (2017).
50. Noback, M., Zhang, G., White, N., Barrow, J. C. & Carr, G. V. Post-weaning social isolation increases ΔFosB/FosB protein expression in sex-specific patterns in the prelimbic/infralimbic cortex and hippocampus in mice. *Neurosci. Lett.* **740**, 135423 (2021).
51. Gold, P. E., Countryman, R. A., Dukala, D. & Chang, Q. Acetylcholine release in the hippocampus and prelimbic cortex during acquisition of a socially transmitted food preference. *Neurobiol. Learn. Mem.* **96**(3), 498–503 (2011).
52. Jorgenson, L. A., Wobken, J. D. & Georgieff, M. K. Perinatal iron deficiency alters apical dendritic growth in hippocampal CA1 pyramidal neurons. *Dev. Neurosci.* **25**(6), 412–420 (2003).
53. Yoo, Y. E., Hong, J. H., Hur, K. C., Oh, E. S. & Chung, J. M. Iron enhances NGF-induced neurite outgrowth in PC12 cells. *Mol. Cells.* **17**(2), 340–346 (2004).
54. Singh, G. et al. Dose- and sex-dependent effects of phlebotomy-induced anemia on the neonatal mouse hippocampal transcriptome. *Pediatr. Res.* **92**(3), 712–720 (2022).

Author contributions

Ao Ding carried out all the experiments, data collection and analyses, and wrote the manuscript. Ting Tan, and Peng Liu participated all the experiments, experimental design, data analyses, and manuscript editing. Xin Li, Mingwei Zhu and Hongsheng Liu participated parts of the studies. Ying Wang provided the technical support. Yuan Chen guided the studies. Ya-Ping Tang guided the studies, and provided the financial support.

Funding

This study was supported by the Guangzhou Health Care Cooperative Innovation Major Project, China (Grant No.201704020221).

Declarations

Competing interests

The authors declare no competing interests.

Ethical approval and consent to participate

All animal experiments (including the rat euthanasia procedure) were conducted following the Guide for the Care and Use of Laboratory Animals. Animal experiments were approved by the Institutional Animal Care and Use Committee of Guangzhou Women and Children's Medical Center.

Additional information

Supplementary Information The online version contains supplementary material available at https://doi.org/10.1038/s41598-026-36710-z.

Correspondence and requests for materials should be addressed to Y.C. or Y.-P.T.